

Microstructure and Mechanical Properties of As-aged Mg-Gd-Zn-Zr-Ag Alloy with Different Contents of Al and Li

Tu Teng¹, Chen Xianhua^{1,2}, Zhang Lijuan¹, Luo zhu¹, Pan Fusheng¹

¹ International Joint Laboratory for Light Alloys (Ministry of Education), Chongqing University, Chongqing 400045, China; ² National Engineering Research Center for Magnesium Alloys, Chongqing 400044, China

Abstract: Microstructure evolution and mechanical properties of Mg-12Gd-1Zn-0.5Zr-0.5Ag (wt%) alloys with different contents of Al and Li elements after T6 heat treatment were investigated. The results indicate that after T6 heat treatment, new Mg₃Gd particles are precipitated in Mg-12Gd-1Zn-0.5Zr-0.5Ag alloy, and most Al₂Li₃ phases in Mg-12Gd-4Al-3Li-1Zn-0.5Zr-0.5Ag and Mg-12Gd-6Al-5Li-1Zn-0.5Zr-0.5Ag alloys become smaller and more evenly distributed. The grain size and *c/a* ratio values of the as-aged Mg-12Gd-4Al-3Li-1Zn-0.5Zr-0.5Ag alloy and Mg-12Gd-6Al-5Li-1Zn-0.5Zr-0.5Ag alloy decrease significantly compared to those of as-aged Mg-12Gd-1Zn-0.5Zr-0.5Ag alloy, which results in improved tensile strength and plasticity. The as-aged Mg-12Gd-6Al-5Li-1Zn-0.5Zr-0.5Ag alloy possesses the best combination of tensile strength, elastic modulus and plasticity, whose ultimate tensile strength, elastic modulus and ductility are 210 MPa, 50.7 GPa and 24.8%, respectively.

Key words: Mg alloy; tensile strength; plasticity; elastic modulus

Over the past decade, the use of structural lightweight magnesium (Mg) alloys in aerospace and transportation sectors has attained an increasing interest because of their high specific strength, excellent electromagnetic shielding and low density^[1-3]. It has been reported that alloying with rare earth (RE) elements can enhance strength of Mg alloys through remarkable solute and second phase strengthening. Elements, such as Zn^[4], Ag^[5,6], or Mn^[7], are often added to Mg-RE (especially Gd or Y)^[8] alloys to improve the age-hardening response. However, the plasticity of high strength Mg-Gd alloys is generally low. For example, the addition of 1% Zn to Mg-8.1Gd-3.8Y-0.4Zr alloy can enhance the strength, but the elongation is only 4.5%^[9]. The addition of 1.8% Ag to Mg-15.6Gd-0.4Zr (wt%) alloy can significantly improve the age-hardening response, but the elongation is less than 2.6%^[5]. As a result, most second precipitates enhance the strength of Mg-RE alloys at the cost of plasticity. Mg alloys exhibit low plasticity because of its hcp (hexagonal close packed) structure and lack of non-basal slip system, so the deformation

of Mg alloys is mainly realized by basal $\langle a \rangle$ slip and $\{10\bar{1}2\} \langle 10\bar{1}1 \rangle$ tensile twin, while the activation of non-basal slip is usually difficult^[10,11].

The key to improve the plasticity of Mg alloys is to decrease the grain size or to activate the non-basal slip. Recently, numerous studies have shown that Li element added to Mg alloys can reduce the crystal axial ratio and activate non-basal slip, which contribute to the improvement of Mg alloy plasticity^[12-14]. In addition, researchers have found that the Mg-Li alloy exhibits excellent tensile properties by adding Al element since Al element can reduce the grain size^[15,16]. Therefore, based on the abovementioned principles, the multi-microalloying technology was introduced to design high plasticity Mg-Gd alloys in our previous study^[17]. Adding Al and Li elements to Mg-Gd-Zn-Ag-Zr alloys can achieve higher plasticity. At the same time, it is found that the addition of Al and Li elements makes the alloys have higher elastic modulus. However, the microstructure and mechanical properties of the alloys after T6 heat treatment have seldom

Received date: February 25, 2020

Foundation item: National Key R & D Program of China (2016YFB0301100); National Natural Science Foundation of China (51571043); Fundamental Research Funds for the Central Universities (2018CDJDCL0019, cqu2018CDHB1A08, 2018CDGFCL0005)

Corresponding author: Chen Xianhua, Ph. D., Professor, College of Materials Science and Engineering, Chongqing University, Chongqing 400045, P. R. China, Tel: 0086-23-65102633, E-mail: xhchen@cqu.edu.cn

Copyright © 2021, Northwest Institute for Nonferrous Metal Research. Published by Science Press. All rights reserved.

been explored yet, so this research mainly study the micro-structure and mechanical properties of aged Mg-Gd-Zn-Zr-Ag with different contents of Al and Li elements.

1 Experiment

Three kinds of Mg-12Gd-1Zn-0.5Ag-0.5Zr (wt%) alloys which contain different amounts of aluminum and lithium were named as alloy 1, alloy 2, alloy 3, respectively. The chemical compositions of alloys are shown in Table 1. These alloys were synthesized from purity Mg (99.98%), Al (99.97%), Li (99.99%), Zn (99.98%), Ag (99.96%), Mg-30%Gd and Mg-30%Zr master alloys by vacuum melting under the protection of Ar atmosphere and the vacuum of 1.85×10^{-2} kPa. The melt was stored at 710 °C for 14~16 min and then cooled in water to form as-cast specimens. Finally, T6 heat treatment was performed: the as-cast specimens were homogenized at 450 °C for 5 h and cooled to room temperature in the furnace, and then aged at 200 °C for 8 h.

The tensile test was conducted using dog-bone specimens with 20 mm in gauge length and 10 mm×2 mm cross-sectional area by a CMT5105 material testing instrument at a tensile strain rate of 1 mm/min. Dynamic young's modulus of specimens was tested by impulse excitation technique in a graphite furnace (HTVP 1750C, IMCE, Diepenbeek, Belgium) at a heating rate of 3 °C/min in Ar atmosphere, the modulus was calculated from the flexural resonant frequency according to ASTM 1876-97, and the surface of 40 mm×15 mm×3 mm specimens were polished to mirror-finish. Nano-modulus of the second phases was tested by nano-indentation machine (Hysitron

Triboindenter) with a Berkovich indenter; the loading and unloading speed was 50 μN/s and the peak load was 300 μN.

An optical microscope (OM), a JEOL JSM-7800F field emission scanning electron microscope (SEM) equipped with an energy dispersive X-ray spectrometer (EDS), a backscatter electron detector (BSE), a HKL Chanel 5 electron back-scattered diffraction (EBSD, TESCAN VEGA2) system with a scan step-size of 0.7 μm, and a transmission electron microscopy (TEM, TECNAI G2 F20) with an accelerating voltage of 200 kV were used to analyze the microstructures. The polished specimens for OM and SEM characterization were etched in 4% nitric acid alcohol; the 3 mm×5 mm×2 mm block specimens for EBSD characterization were polished by Ar-ion Gatan 697 system; the foil specimens for TEM characterization were milled by Ar-ion Gatan 695 system. The average linear intercept method was used to test grain size and X-ray diffraction (XRD) with Cu Kα radiation at 60 kV and 30 mA was used for phase analysis.

2 Results and Discussion

2.1 Microstructures

The OM and SEM-BSE images of as-cast alloy1 are shown in Fig.1a and 1b, respectively. In Fig.1a, the eutectic phases A

Table 1 Chemical compositions of alloys (wt%)

Alloy	Gd	Zn	Ag	Zr	Al	Li	Mg
1	12	1	0.5	0.5	0	0	Bal.
2	12	1	0.5	0.5	4	3	Bal.
3	12	1	0.5	0.5	6	5	Bal.

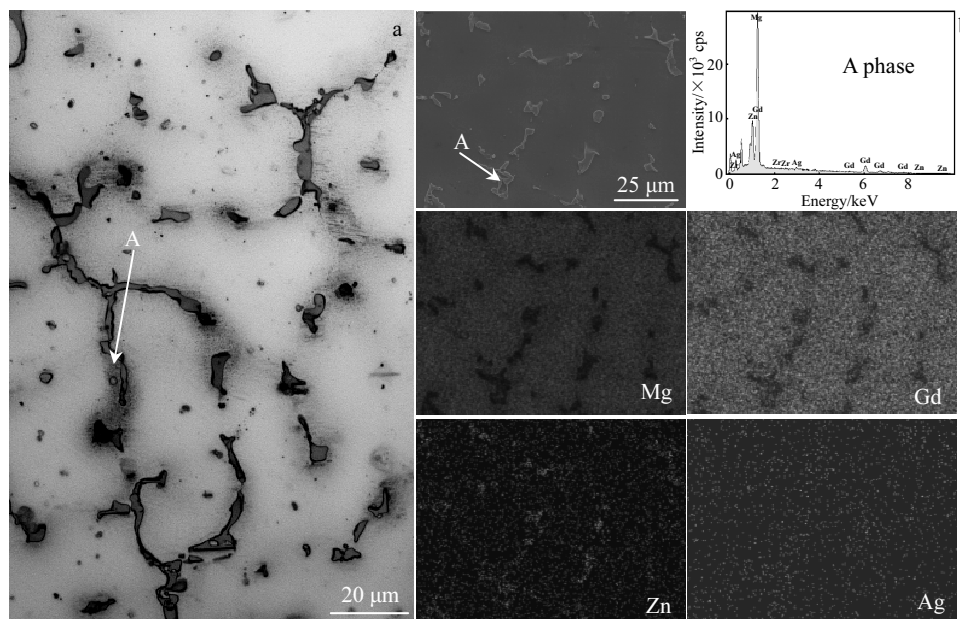


Fig.1 OM image of the as-cast alloy 1 (a); SEM-BES image, EDS spectrum of A phase and corresponding elemental mappings of Mg, Gd, Zn, Ag in as-cast alloy 1 (b)

(marked with the white arrow) are discontinuously distributed in network. By EDS analysis of A phase shown in Fig.1b, the A phase consists of Mg, Gd and Zn. The elemental mappings show that Ag element is evenly distributed in magnesium matrix. According to the results of Ref.[17], the A phase is $(\text{Mg, Zn})_3\text{Gd}$ compound. Fig.2a and 2b show the OM and SEM-BSE images of as-cast alloy 2, respectively. Compared with the as-cast alloy 1, the grain boundaries (Fig.2a) of the as-cast alloy 2 is clear due to the alloying of Al element, and the second phase is mainly gray block phase C and round particle D. The elemental mappings indicate that Al element has obvious segregation in C and D phases, and the EDS data of C position in SEM-BES image (Fig.2b) show that the C phase consists of Gd and Al; combined with the results in Ref.[17], C phase is Al_2Gd phase. The OM and SEM-BSE images of as-cast alloy 3 are shown in Fig.3a and 3b, respectively. As the Al and Li content increase, there is still gray block phase C, but the black round particle D increases to form black regions. The corresponding study^[17] shows that the black round particle is Al_2Li_3 phase. The elemental mappings indicate that Al element has obvious segregation in D phase, and the Li element is too light to detect, so the D phase in as-cast alloy 3 should be Al_2Li_3 particles.

After T6 heat treatment, the X-ray diffraction (XRD) patterns of the as-aged alloy 1, alloy 2 and alloy 3 are shown in Fig.4. Alloy1 presents $(\text{Mg, Zn})_3\text{Gd}$ and Mg_3Gd phases, and

with the addition of Al and Li, Al_2Gd and Al_2Li_3 phases form in alloy 2 and alloy 3. Fig.5a shows the OM image of alloy 1 in the as-aged condition. Compared with the as-cast alloy1, apart from the A phases, as-aged alloy 1 presents some new precipitated particles B. According to the results of XRD, BF-TEM image of A, B phases and corresponding SAED patterns in Fig.5b and 5c, this A phase is $(\text{Mg, Zn})_3\text{Gd}$ and B particle is Mg_3Gd . Similar results have been reported in Ref.[18,19]. This indicates that a new Mg_3Gd phase is precipitated in alloy 1 after T6 heat treatment. Fig.6a and 6b show the OM images of alloy 2 and alloy 3 in the as-aged condition, respectively. Compared with the as-cast alloy 2 and as-cast alloy 3, the as-aged alloy 2 and alloy 3 still have C phases, but most of the D phases dissolve into the matrix after T6 heat treatment. According to the BF-TEM images of C, D phases in as-aged alloy 3 and corresponding SAED patterns in Fig.6c and 6d, these C and D phases are mainly identified as the Al_2Gd and Al_2Li_3 , consistent with the results of XRD (Fig.4). This indicates that most Al_2Li_3 phases in alloy 2 and alloy 3 become smaller and more evenly distributed after T6 heat treatment.

Fig.7 shows the inverse pole figure (IPF) maps of as-aged alloy 1, alloy 2 and alloy 3. The grain orientation in Fig.7a~7c is represented by the color legend. In Fig.7b and 7c, the Al_2Gd and Al_2Li_3 phases are located in the white region, which indicate the region with low confidence index^[20]. The average

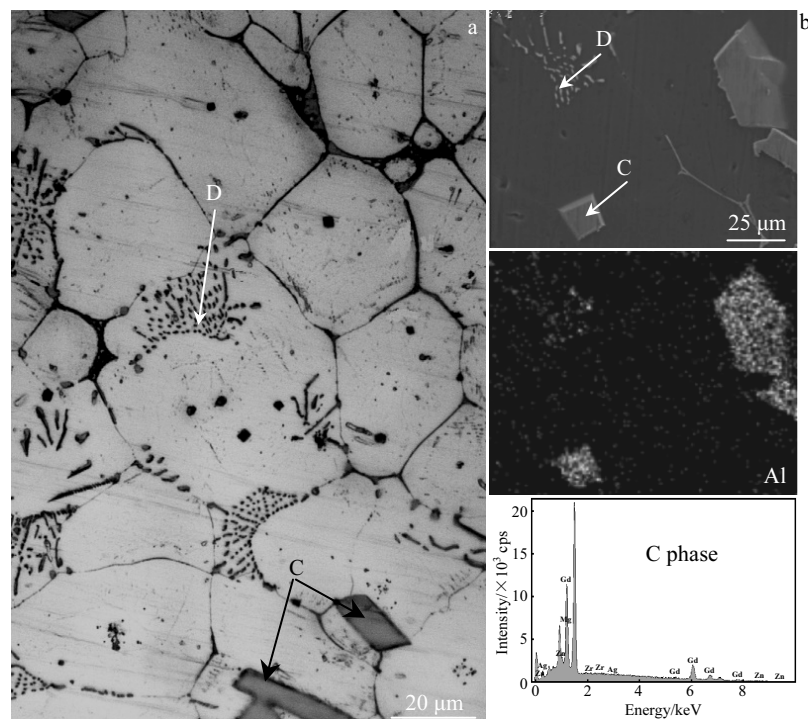


Fig.2 OM image of the as-cast alloy 2 (a); SEM-BES image, EDS spectrum of C phase and corresponding elemental mapping of Al in as-cast alloy 2 (b)

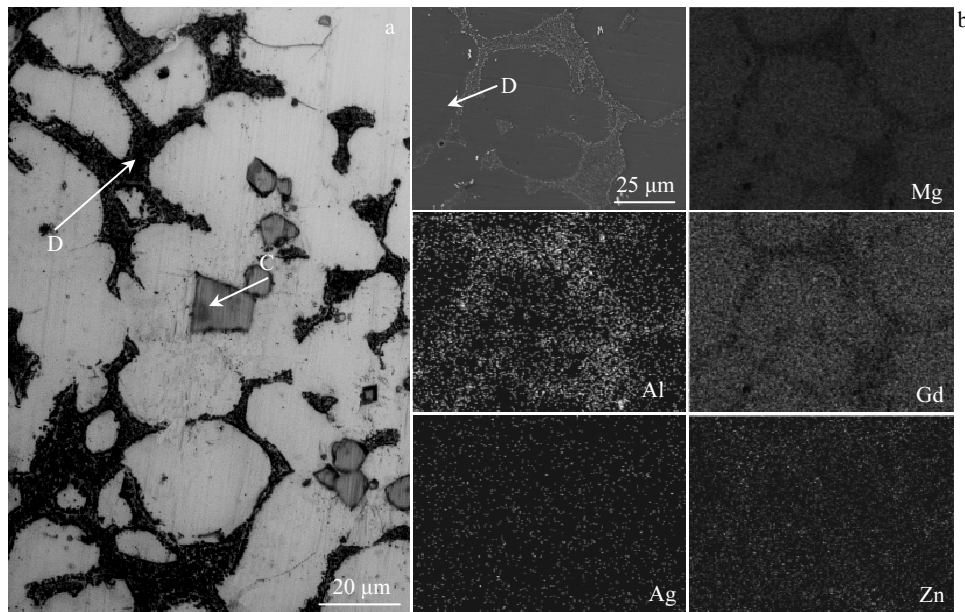


Fig.3 OM image of the as-cast alloy 3 (a); SEM-BES image and corresponding elemental mappings of Mg, Al, Gd, Ag, Zn in as-cast alloy 3 (b)

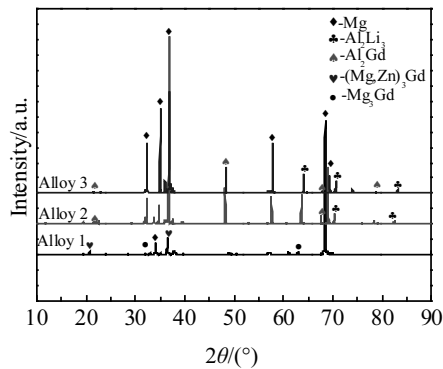


Fig.4 XRD patterns of as-aged alloy 1, alloy 2, and alloy 3

grain size of as-aged alloy 1 is approximately 237.8 μm , while that of as-aged alloy 2 and alloy 3 decreases significantly to 32.4 and 25.56 μm , respectively. This is because Al element plays a refining grains role in Mg alloys, which is consistent with the previous report^[21-23], revealing that Al has a segregating effect in the Mg alloy.

2.2 Tensile strength

Fig.8 exhibits the engineering stress-strain curves of the as-aged alloy 1, alloy 2 and alloy 3. The ultimate tensile strengths (UTS) of the as-aged alloy 1, alloy 2 and alloy 3 are 170, 188 and 210 MPa, respectively; the yield stresses (YS) of the as-aged alloy 1, alloy 2 and alloy 3 are 94, 104 and 119 MPa, respectively. As the content of Al and Li increases, the Al- and Li-containing alloys exhibit stronger precipitation hardening response than Al- and Li-free alloy. It is mainly due

to fine grain strengthening and second phase strengthening. On the one hand, fine grain is one of the key parameters influencing the tensile strength of Mg alloys. As shown in Fig.7, the grain size of as-aged alloy 1 is 237.8 μm ; when Al content increases to 4%, the grain size of as-aged alloy 2 is refined to 32.4 μm ; when Al content increases to 6%, the grain size of as-aged alloy 3 is refined to 25.56 μm . Compared with the as-aged alloy 1, the UTS and YS of as-aged alloy 2 and alloy 3 increase gradually with the decrease of grain size. The Hall-Petch equation^[24] $\sigma_s = \sigma_0 + kd^{-1/2}$ can represent the relationship between the grain size and the yield strength (σ_s is the yield strength, σ_0 is the friction stress for dislocation movement, k is the strength coefficient for the normal stress and d is the grain size). The reduction of grain size increases the tensile strength, and as a result, the dislocations are stuck at the grain boundaries and greater stress is needed to release the dislocations from obstacles. This is why the tensile strength of Al- and Li-containing alloys increases with the decrease of grain size.

On the other hand, the amount of secondary phases in Al- and Li-containing alloys gradually increases, as shown in Fig.5a and Fig.6a and 6b. Especially in as-aged alloy 3, it can be seen that a large amount of particles are precipitated inside the grain or at the grain boundary. The pinning effect of particles restricts the growth of recrystallized grain, which can be regarded as obstacles to the grain boundaries^[25,26]. Thus, the increase in the amount of second phases leads to the grain refinement, which increases the strength of Al- and Li-containing alloys.

2.3 Plasticity

As shown in Fig.8, the ductility of the as-aged alloy 1,

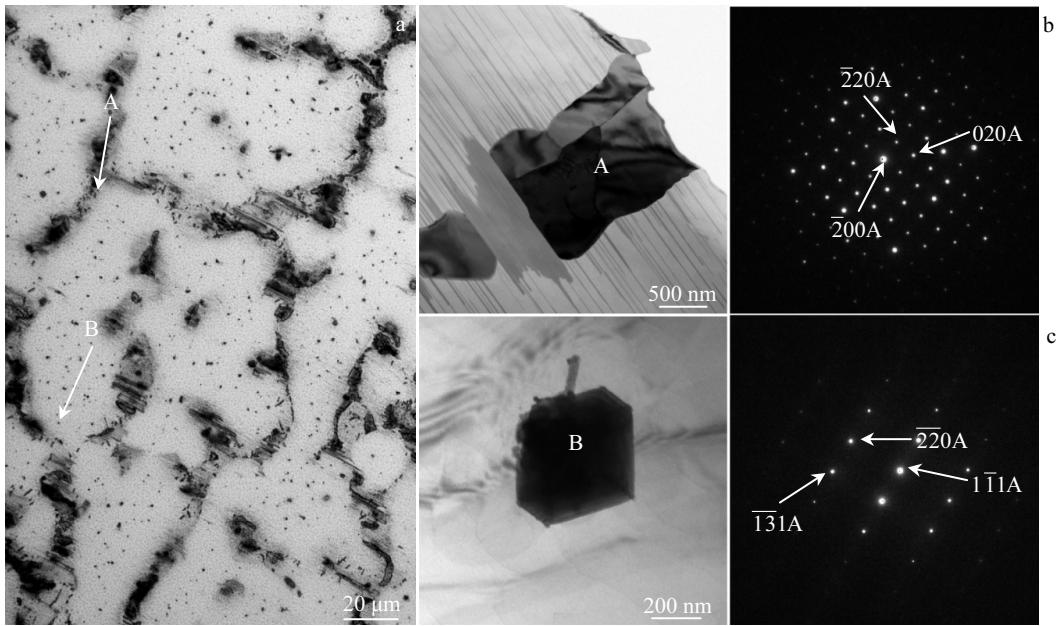


Fig.5 OM image of as-aged alloy 1 (a); BF-TEM image of A phase and corresponding SAED pattern (b) and BF-TEM image of B phase and corresponding SAED pattern (c) of as-aged alloy 1

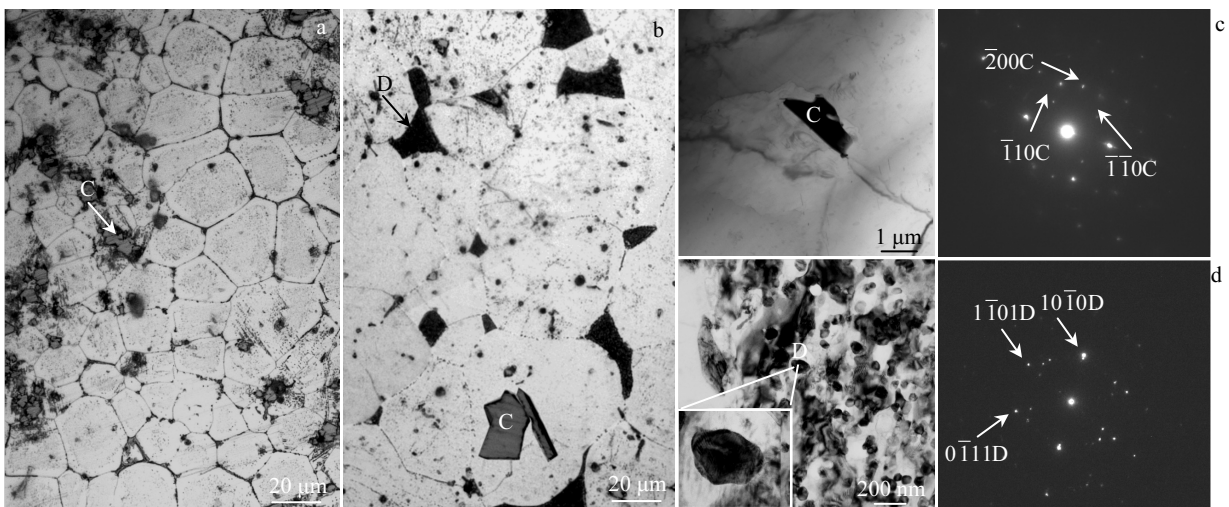


Fig.6 OM image of as-aged alloy 2 (a) and alloy 3 (b); BF-TEM image of C phase and corresponding SAED pattern (c) and BF-TEM image of D phase and corresponding SAED pattern (d) of as-aged alloy 3

alloy 2 and alloy 3 are 4.6%, 11.8% and 24.8%, respectively. The higher the contents of Al and Li in the alloys, the better the ductility of the alloys. This is mainly summarized as the following three factors. Firstly, fine grain can not only improve the tensile strength of Mg alloy, but also improve its ductility. Compared with as-aged alloy 1, the ductility of as-aged alloy 2 and alloy 3 gradually increases with the decrease of grain size. This is because the fine grain of Al- and Li-containing alloys leads to the reduction of stress

concentration while the grain boundary increases, and the non-basal slip near grain boundary is easily activated, which is beneficial to the improvement of plasticity.

Secondly, by statistics^[27], the addition of Li can activate the non-basal slip and reduce the crystal axial c/a ratio of Mg alloys, thus increasing the ductility. In this work, the c/a ratios of as-aged alloy 1, alloy 2 and alloy 3 are calculated by XRD analysis to be 1.624, 1.621 and 1.619, respectively. The c/a ratio of as-aged alloy 3 with higher Li contents is much lower,

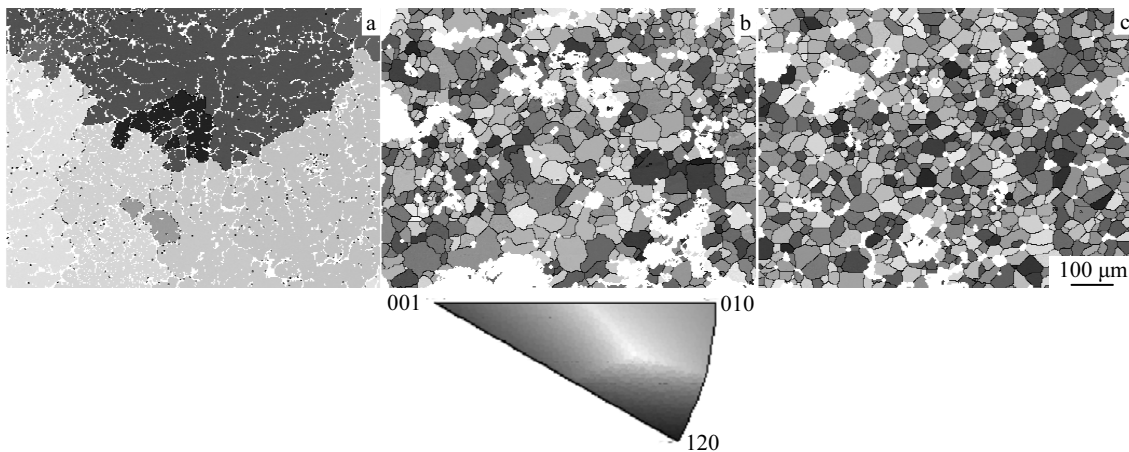


Fig.7 Inverse pole figure (IPF) maps of as-aged alloy 1 (a), alloy 2 (b) and alloy 3 (c)

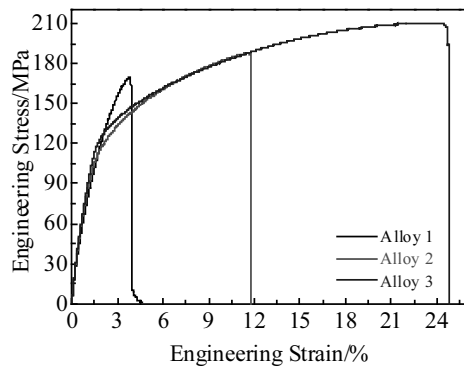


Fig.8 Tensile engineering stress-strain curves of as-aged alloy 1, alloy 2 and alloy 3

which indicates that the reduction in c/a ratio contributes to the improvement in ductility. Furthermore, in order to identify whether the addition of Li to alloy 2 and alloy 3 can operate non-basal slip, visco-plastic self-consistent (VPSC) model was carried in this work, which was used to simulate the plastic deformation process of as-aged alloy 1, alloy 2 and alloy 3 and to predict the relative activities of various slip systems according to the voce hardening equation^[28]. Fig.9a shows that the simulated results (dotted lines) by VPSC model are well fitted with the solid lines of true stress-strain curves by experiment. Fig.9b~9d show the relative activities of different deformation modes during the tensile process of the as-aged alloy 1, alloy 2 and alloy 3. Basal slip is the main deformation mode in the as-aged alloy 1, alloy 2 and alloy 3. The difference is that basal $\langle a \rangle$ slip and prismatic $\langle a \rangle$ slip are activated in as-aged alloy1. But as the content of Al and Li increases to 4% and 3% in as-aged alloy 2, except basal $\langle a \rangle$ slip and prismatic $\langle a \rangle$ slip, pyramidal $\langle c+a \rangle$ slip is gradually activated at the plastic strain of 2%. Moreover, as the content

of Al and Li increases to 6% and 5% in as-aged alloy 3, the pyramidal $\langle c+a \rangle$ slip is immediately activated from the first stage of plastic deformation. This indicates that the non-basal slips of pyramidal $\langle c+a \rangle$ slip in as-aged alloy 2 and alloy 3 are rapidly activated due to the increased Li content compared with as-aged alloy 1, and the activation of pyramidal $\langle c+a \rangle$ slip in as-aged alloy 3 is higher than in alloy 2, which helps to the improvement of the ductility of as-aged alloy 3.

2.4 Elastic modulus

Elastic modulus is usually a measure of the stiffness or resistance of a material to elastic deformation, and the greater the elastic modulus of a metal, the stiffer it becomes^[29]. Modulus depends essentially on the type of interatomic binding forces, that is, the metallic bonding prevails in alloys. The nominal elastic modulus of pure Mg is 45 GPa, and the researchers reported experimental values range from 39 GPa to 45 GPa^[30]. In this work, according to the impulse excitation testing, elastic modulus of the as-aged alloy 1, alloy 2 and alloy 3 are 44.9 ± 0.1 , 49.9 ± 0.2 , and 50.7 ± 0.4 GPa, respectively are shown in Fig.10a. Compared with pure Mg and as-aged alloy 1, the modulus of as-aged alloy 2 and alloy 3 are significantly improved. This is because the elastic modulus of Mg alloys is mainly determined by the elastic modulus and volume fractions of its constituent phases^[31]. Therefore, the elastic modulus of the matrix region with Al_2Li_3 and Al_2Gd phases in the as-aged alloy 3 is studied by nano-indentation test. The indentation size is about 70 nm, smaller than that of each phase. Fig.10b and 10c show the elastic modulus and load-depth curves of α -Mg, Al_2Li_3 and Al_2Gd phase in as-aged alloy 3. The result shows that elastic modulus is 45.0 ± 2.5 GPa for matrix, 66.3 ± 1.9 GPa for Al_2Li_3 phase and 75.5 ± 1.8 GPa for Al_2Gd phase, and the elastic modulus and stiffness order of the three phases is α -Mg matrix $< \text{Al}_2\text{Li}_3 < \text{Al}_2\text{Gd}$, which is consistent with the elastic modulus of the three phases calculated by first principles calculation in Ref.[17]. Thus, the

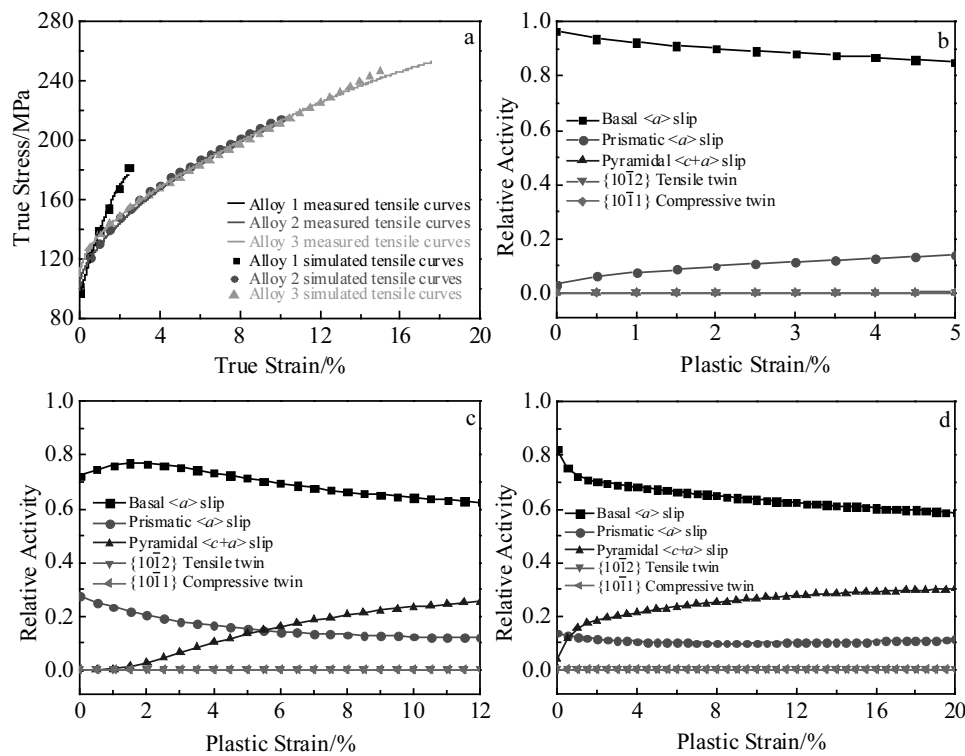


Fig.9 True stress-strain curves and corresponding simulated curves of as-aged alloy 1, alloy 2 and alloy 3 (a); relative activities of different slip models during uniaxial tensile of as-aged alloy 1 (b), alloy 2 (c) and alloy 3 (d)

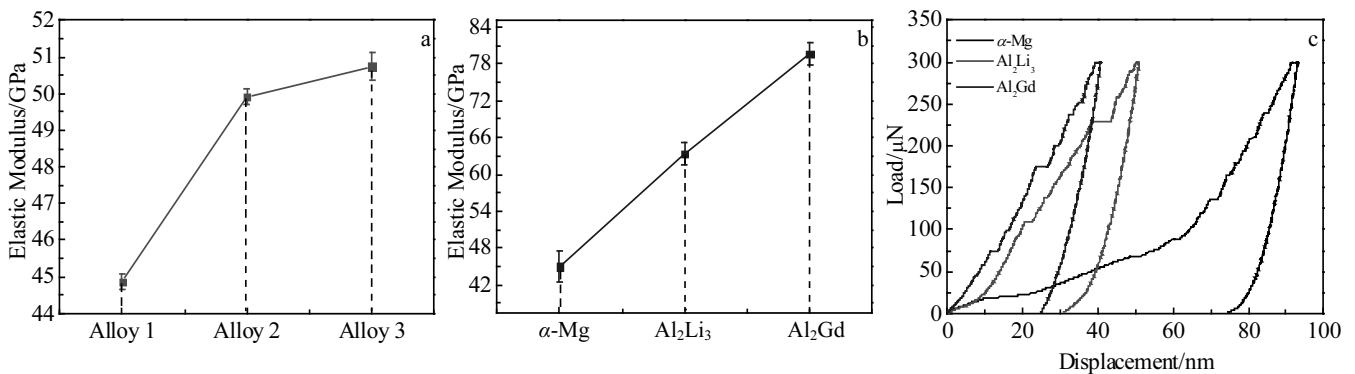


Fig.10 Elastic modulus of the as-aged alloy 1, alloy 2 and alloy 3 (a); Elastic modulus of the α -Mg, Al_2Li_3 and Al_2Gd phase in as-aged alloy 3 (b); and their corresponding load-depth curves (c)

elastic modulus of as-aged alloy 2 and alloy 3 is higher than that of pure Mg and as-aged alloy 1, which is attributed to the presence of high-modulus Al_2Gd and Al_2Li_3 phases.

2.5 Comprehensive properties comparison

Table 2 summarizes the reported mechanical properties of Mg based alloys (no deformation processing) in comparison with the alloys in this work. On the one hand, under the absence of deformation processing, the elongation of as-aged alloy 3 in this work is significantly higher than that of Mg alloys^[23,32,33], and the strength and plasticity are greatly

enhanced compared with the commonly used AZ31 and AZ91D alloys. On the other hand, modulus and plasticity are usually the opposite parts, as shown by the high modulus Mg matrix composites^[33,34], the smaller the modulus value, the better the plasticity. The modulus of as-aged alloy 2 and alloy 3 in this work is much higher than that of the commonly used AZ31 alloy and slightly lower than the Mg matrix composites^[33,34], but plasticity is far greater than that of the Mg matrix composites, which breaks the balance of smaller modulus with better plasticity. Thus, the as-aged alloy 3 in this

Table 2 Comparison of reported mechanical properties of Mg based alloys (no deformation processing) with alloys in this work

Alloy	State	UTS/MPa	YS/MPa	Elongation/%	Modulus/GPa	Refs.
Alloy 2	T6	188±2	104±1	11.8±1.3	49.9±0.2	This work
Alloy 3	T6	210±3	119±2	24.8±0.9	50.7±0.4	This work
AZ31	T4	169	58	8.2	-	[32]
Mg-8.0Zn-1.0Al-0.5Cu-0.5Mn	T6	325	260	17.0	-	[23]
AZ91D	Cast	128	86	0.9	44.3	[33]
1.5%CNTs/AZ91D	Cast	157	104	1.38	64.3	[33]
33%Mg2B2O5W/AZ91D	Cast	265	262	0.95	54.0	[34]

work has the comprehensive properties of good tensile strength, high plasticity and high elastic modulus.

3 Conclusions

1) Compared with as-cast Mg-12Gd-1Zn-0.5Zr-0.5Ag (alloy 1), in addition to the (Mg, Zn)₃Gd phase, new particles Mg₃Gd are precipitated from as-aged alloy 1. The Al₂Gd phases of Mg-12Gd-4Al-3Li-1Zn-0.5Zr-0.5Ag (alloy 2) and Mg-12Gd-6Al-5Li-1Zn-0.5Zr-0.5Ag (alloy 3) both in as-cast condition and as-aged condition have no change, but most Al₂Li₃ phase in as-aged alloy 2 and alloy 3 becomes smaller and more evenly distributed than that in as-cast alloy 2 and alloy 3.

2) The grain size and *c/a* ratio values of the as-aged alloy 2 and alloy 3 decrease significantly compared to those of as-aged alloy 1, which is beneficial to plasticity and tensile strength.

3) Compared with other un-deformed Mg based alloys, the as-aged alloy 3 possesses the best combination of tensile properties, plasticity and elastic modulus, whose ultimate tensile strength, elastic modulus and ductility are 210 MPa, 50.7 GPa and 24.8%, respectively.

References

- Janbozorgi M, Taheri K K, Taheri A K. *Journal of Magnesium and Alloys*[J], 2019, 7(1): 80
- Javaid A, Czerwinski F. *Journal of Magnesium and Alloys*[J], 2019, 7(1): 27
- Zhao C Y, Chen X H, Pan F S et al. *J. Journal of Materials Science & Technology*[J], 2019, 35(1): 142
- Li J C, He Z L, Fun P H et al. *Materials Science and Engineering A*[J], 2016, 651(10): 745
- Zhang Y, Wu Y J, Peng L M et al. *Journal of Alloys and Compounds*[J], 2014, 615(5): 703
- Wang J f, Wang K, Hou F et al. *Materials Science and Engineering A*[J], 2018, 728(13): 10
- Heng X W, Zhang Y, Rong W et al. *Materials & Design*[J], 2019, 169(5): 107
- Zhang J H, Liu S J, Wu R Z et al. *Journal of Magnesium and Alloys*[J], 2018, 6(3): 277
- Xu C, Zheng M Y, Xu S W et al. *Materials Science and Engineering A*[J], 2012, 547(15): 93
- Zhu G M, Wang L Y, Zhou H et al. *International Journal of Plasticity*[J], 2019, 120: 164
- Tu T, Chen X H, Chen J et al. *Acta Metallurgica Sinica (English Letters)*[J], 2019, 32(1): 23
- Kumar V, Govind, Shekhar R et al. *Materials Science and Engineering A*[J], 2012, 547(15): 38
- Xu T C, Peng X D, Jiang J W et al. *Rare Metal Materials and Engineering* [J], 2014, 43(8): 1815
- Zhou W R, Zheng Y F, Leeftang M A et al. *Acta Biomaterialia* [J], 2013, 9(10): 8488
- Rahulani N, Gopalan S, Kumaran S. *Materials Today: Proceedings*[J], 2018, 5(9): 17 935
- Xiao H, Zhen L Z, Zhang K F et al. *Materials & Design*[J], 2020, 186(15): 108
- Tu T, Chen X H, Zhao C Y et al. *Materials Science and Engineering A*[J], 2020, 771(13): 138
- Wen K, Liu K, Wang Z H et al. *Materials Science and Engineering A*[J], 2016, 674(30): 33
- Rong W, Zhang Y, Wu Y J et al. *Materials Characterization*[J], 2017, 131: 380
- Zhao D, Chen X H, Ye J L et al. *Journal of Alloys and Compounds*[J], 2019, 810 (25): 151
- Park G H, Kim J T, Park H J et al. *Journal of Alloys and Compounds*[J], 2016, 680(25): 116
- Park S S, Bae G T, Kang D H et al. *Scripta Materialia*[J], 2007, 57(9): 793
- Wang J, Liu R D, Luo T J et al. *Materials & Design*[J], 2013, 47: 746
- Wang Q H, Shen Y Q, Jiang B et al. *Materials Science and Engineering A*[J], 2018, 735(26): 131
- Langelier B, Nasiri A M, Lee S Y et al. *Materials Science and Engineering A*[J], 2015, 620(3): 76
- Fu H, Liu N, Zhang Z W et al. *Journal of Magnesium and Alloys*[J], 2016, 4(4): 302
- Tang Y, Jia W T, Liu X et al. *Materials Science and Engineering A*[J], 2017, 689(24): 332
- Zhao L Y, Chapuis A, Xin Y C et al. *Journal of Alloys and Compounds*[J], 2017, 710(5): 159
- Jiang W, Zou C M, Huang H T et al. *Journal of Alloys and Compounds*[J], 2017, 717(15): 214
- Peng Q M, Meng J, Li Y D et al. *Materials Science and Engineering A*[J], 2011, 528(4-5): 2106
- Li P, Hao J Y, Zhao J et al. *Materials Science and Engineering A*[J], 2010, 527(29-30): 7469

- 32 Peng Q M, Huang Y D, Kainer K U et al. *Materials Letters*[J], 2012, 83(15): 209
- 33 Liu S Y, Gao F P, Zhang Q Y et al. *Transaction of Nonferrous Metals Society of China*[J], 2010, 20(7): 1222
- 34 Liu G J, Li W F, Ma L J et al. *Acta Material Composite Sinica*[J], 2008, 25(6): 1000 (in Chinese)

Al 和 Li 含量不同的时效态 Mg-Gd-Zn-Zr-Ag 合金的组织 and 力学性能

涂 腾¹, 陈先华^{1,2}, 张利娟¹, 罗 铸¹, 潘复生¹

(1. 重庆大学 轻合金国际联合实验室(教育部), 重庆 400045)

(2. 国家镁合金工程技术研究中心, 重庆 400044)

摘 要: 研究了铝和锂元素含量不同的 Mg-12Gd-1Zn-0.5Zr-0.5Ag (质量分数, %)合金经 T6 热处理后的组织演变和力学性能。结果表明, T6 热处理后, 有新的 Mg₃Gd 颗粒从 Mg-12Gd-1Zn-0.5Zr-0.5Ag 合金中析出, 且 Mg-12Gd-4Al-3Li-1Zn-0.5Zr-0.5Ag 和 Mg-12Gd-6Al-5Li-1Zn-0.5Zr-0.5Ag 合金中的大多数 Al₂Li₃ 相变得更细小, 分布更均匀。时效态 Mg-12Gd-4Al-3Li-1Zn-0.5Zr-0.5Ag 和 Mg-12Gd-6Al-5Li-1Zn-0.5Zr-0.5Ag 合金中的晶粒尺寸和 c/a 比值相比时效态 Mg-12Gd-1Zn-0.5Zr-0.5Ag 合金有显著的减小, 这有利于提高抗拉强度和塑性。时效态 Mg-12Gd-6Al-5Li-1Zn-0.5Zr-0.5Ag 合金具有最佳的抗拉强度、弹性模量和塑性匹配, 其抗拉强度为 210 MPa, 弹性模量为 50.7 GPa, 延性率为 24.8%。

关键词: 镁合金; 抗拉强度; 塑性; 弹性模量

作者简介: 涂 腾, 女, 1991 年生, 博士, 重庆大学材料科学与工程学院, 重庆 400045, 电话: 023-65102366, E-mail: cqliu@cqu.edu.cn